Dependency of Inner Liner Surface Temperature on Coolant Mass Flow Rate and Heat Flux in Rocket Combustion Chambers

SPACE PROPULSION 2020+1

17 - 18 - 19 MARCH 2021

Pascal H. Kringe[1,6], Jörg R. Riccius[1], Evgeny Zametaev[1], Michael Oschwald[1,2], Andreas Gernoth[3], Sebastian Soller[4], Marcus Lehmann[4] and Stefanie Reese[5]

[1] *German Aerospace Center (DLR), Institute of Space Propulsion, 74239 Lampoldshausen, Germany*
[2] *RWTH Aachen University, Institute of Jet Propulsion and Turbomachinery, Aachen, Germany*
[3] *ESA ESTEC Noordwijk, The Netherlands*
[4] *ArianeGroup GmbH, Munich, Germany*
[5] *Institute of Applied Mechanics, RWTH Aachen University, Aachen, Germany*
[6] *Corresponding author: pascal.kringe@dlr.de*

KEYWORDS: liquid rocket engine combustion chamber, convective heat transfer, Nusselt number, high thermal conductivity copper

ABSTRACT:

This paper presents the experimental results of the dependence of the surface temperature on coolant mass flow rate and heat flux in a high thermal conductivity copper material for regeneratively cooled rocket combustion chambers. The particular material is appropriate for lowly loaded combustion chambers like upper stages. Instead of an experimental rocket combustion chamber, only a small section of a combustion chamber wall of 7 cooling channels, the so-called Heat Transfer Test (HTT) Panel is investigated. Due to safety reasons and cost factors, the HTT Panel is heated by a high power diode laser and cooled with nitrogen. The nitrogen coolant is in supercritical condition with $T = 160$ K and $p = 55$ bar when entering the HTT Panel. The diode laser provides a power output of up to $P = 11$ kW with a top hat intensity of up to $I = 28$ MW/m^2. The heat flux was varied between $\dot{q} = 12$ MW/m^2 to $\dot{q} = 24.6$ MW/m^2. The surface temperature was varied from $T_s = 648$ K to $T_s = 1000$ K and the mass flow range was $\dot{m} = 8.0$ g/s to $\dot{m} = 47.0$ g/s per cooling channel leading to effective Reynolds numbers between $Re = 1 \times 10^5$ to $Re = 5.4 \times 10^5$. The experimental results indicate that for high heat fluxes the coolant mass flow rate has to be increased non-linearly when the surface temperature is kept constant. The data obtained regarding the dependence surface temperature on coolant mass flow rate and heat flux within this experiment is used for evaluation of Nusselt correlations.

1. Introduction

Liquid rocket engines (LRE) are still the state of the art for modern launch systems. One of the most critical components within the engine is the combustion chamber. Regeneratively cooled liquid rocket engines have to withstand extreme temperatures, high temperature gradients and extreme pressure differences. Today new engines are mainly developed using numerical methods including Computational Fluid Dynamics (CFD) and Finite Elemente Analysis (FEA). However, for accurate numerical analyses it is important to validate the underlying algorithms with experimental data. The data presented in this paper was obtained within a pre-study in the framework of a thermomechanical fatigue (TMF) life study for a high-conductivity copper inner liner material jointly conducted by the European Space Agency (ESA), the German Aerospace Center (DLR) and ArianeGroup GmbH. The material is a potential candidate for lowly loaded (regarding hot wall surface temperature and heat flux) upper stage engines. The study used the TMF test bench at DLR Institute of Space Propulsion in Lampoldshausen [1] - [4] to examine the heat transfer properties [5] of the copper material in this particular test setup. These results will be used for the upcoming test campaigns to easily set up the necessary mass flow rates for the envisioned combinations of heat flux and surface temperature and, at a later stage of the project, become important in order to set up and validate a coupled FE-CFD simulation (thermal fluid-structure-interaction (FSI) analysis). Additionally, different Nusselt correlations were evaluated and compared to the experimental data.

2. Experimental Setup

This section describes the experimental setup in detail. Particularly the HTT panel itself as well as the test bench, its components and the measurement and control system are presented.

2.1 Heat Transfer Test Panel

The geometry of the HTT panel was developed by Thiede in [3] with a clear focus on TMF panel tests. It includes seven cooling channels whereof five (2-6) represent the actual cooling channel geometry. Cooling channels 1 and 7 have a slightly larger cross section to effectively

cool down the two side bulks of the HTT panel to induce a stress on the inner cooling channels (2-6) which is comparable to the hoop stress in a LRE. A cross section of the HTT panel is shown in Figure 1 with the relevant parameters shown in Table 1, the overall geometry can be found in Figure 6. The new panel design was

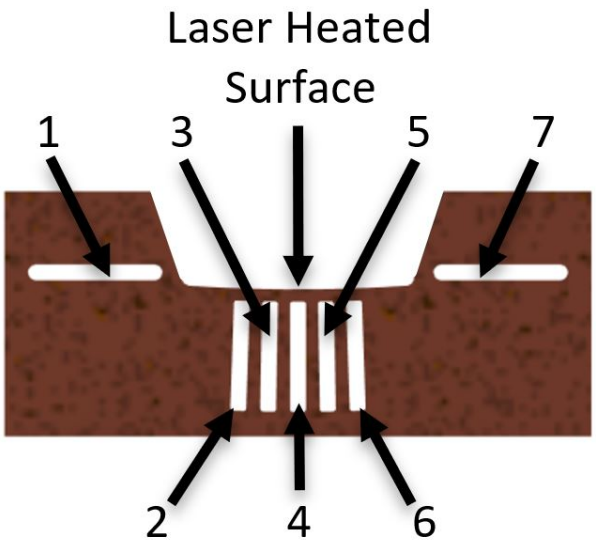

Figure 1: **Cross section of the HTT panel. Cooling channels are numbered from left (1) to right (7).**

Table 1: **Dimensions of the HTT panel**

Total size	$48 \times 230 \times 20$ mm
Number of cooling channels	$5 + 2$
Laser-heated wall thickness	1 mm
Channel width	1.3 mm
Height of channels 2 - 6	9 mm
Angular separation of cooling channels	1°
Laser loaded surface	cylindrical $r = 130$ mm

introduced in the framework of the DLR internal project AKIRA (see [4]). The material used in the work presented here is high conductivity copper. Because copper has a very low emissivity coefficient at the wavelength of the laser (see Table 2) the HTT panel is coated. The coating consists of three layers which are applied by Physical Vapor Deposition (PVD) at Fraunhofer Institute for Material and Beam Technology (IWS). The coating increases the emissivity coefficient at laser wavelength to $\varepsilon_{940\ \mathrm{nm}} = 0.95$. Figure 2 graphically presents the normalized heat conductivity, thermal diffusivity and heat capacity of the HTT panel material which were experimentally determined by Fraunhofer Institute for Mechanics of Materials (IWM).

2.2 Panel Test Bench

The panel test bench at DLR Lampoldshausen consists of three main parts, the control room, the test cell and the

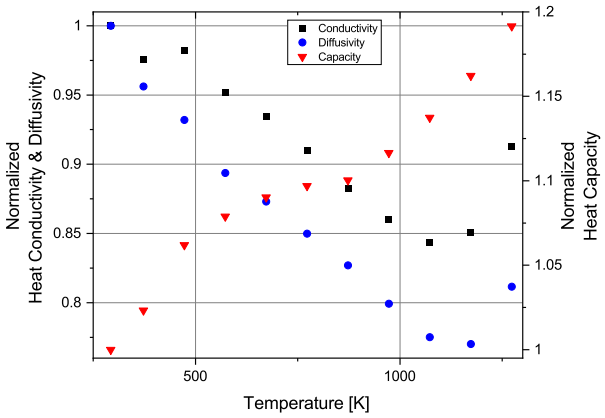

Figure 2: **Normalized properties regarding heat transfer of the HTT panel material.**

fluid supply and dump system. The most relevant parts are described in this section.

High Power Diode Laser System

For a close-to-reality simulation of the exceptionally high heat fluxes through rocket combustion chamber walls (up to $\dot{q}_w = 80\ \mathrm{MW/m^2}$ in the Vulcain II main engine) only a high power diode laser can create adequate heat fluxes on a sufficiently sized focal plane. The diode laser was manufactured by DILAS. It consists of 5 laser modules totaling 2000 diodes with an optical power output of $P = 11$ kW. The beam is focused onto a half width focal plane of $A_{focal} = 11.2\ \mathrm{mm} \times 32.2\ \mathrm{mm}$ (see Fig. 3 to Fig. 5) leading to a top hat intensity of $I = 28\ \mathrm{MW/m^2}$. The technical properties of the laser are summarized in Table 2. The laser output power is controlled via an out-

Table 2: **Technical data of DILAS diode laser**

Parameter	**Symbol**	
Laser wavelength	λ	940 ± 10 nm
Optical power output	P	11 kW
Focal plane size	A	$11.2\ \mathrm{mm} \times 32.2\ \mathrm{mm}$
Focal distance	l	399 mm
Homogeneity		$< \pm 5$ %
Maximum output intensity	I	$28\ \mathrm{MW/m^2}$

put control voltage ranging between $U_{ctrl} = 1.1...6.0$ V. By a series of laser power meter measurement, the following equation was determined between the control voltage and the optical output power of the laser:

$$P_{out} = 2230.1 \frac{\mathrm{W}}{\mathrm{V}}\, U_{ctrl} - 2759.1\mathrm{W} \qquad (1)$$

Hence, the top hat heat flux into the HTT panel can directly be expressed as a function of the output control

voltage

$$\dot{q}_w = 5.5878 \frac{\mathrm{MW}}{\mathrm{m^2 V}} U_{ctrl} - 7.0451 \frac{\mathrm{MW}}{\mathrm{m^2}} \quad (2)$$

by taking into account the relevant top hat area and emissivity coefficient of the coating. For the characterization of the laser, particularly for the evaluation of Equations (1) and (2), a PRIMES Power Monitor and Beam Profiler are available (see [4]).

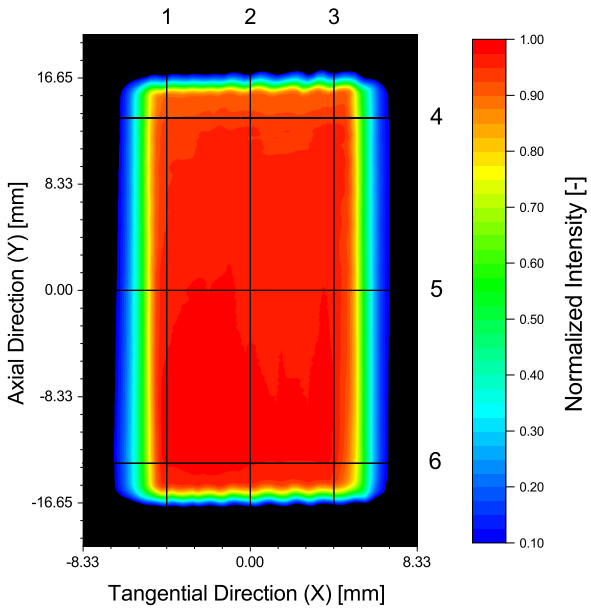

Figure 3: **Normalized laser top hat intensity in the focal plane and** $U_{ctrl} = 5.6$ V

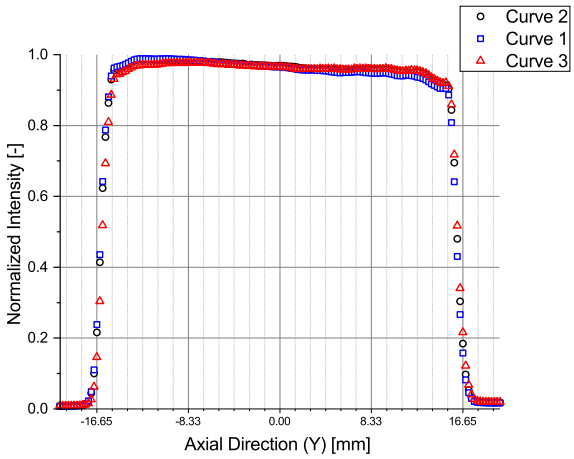

Figure 4: **Cross section of the laser top hat in axial direction (Y) in three representative planes (1-3) marked in Figure 3**

Measurement and Control System

The measurement and control system comprises several subsystems from which only the most relevant are mentioned here.

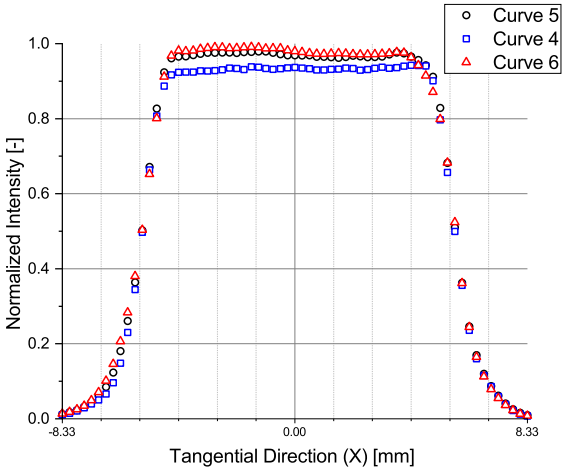

Figure 5: **Cross section of the laser top hat in tangential direction (X) in three representative planes (4-6) marked in Figure 3**

The temperatures and pressures of the fluid inside the HTT panel are measured with eight thermocouples and absolute pressure sensors, respectively, according to the sensor locations in Figure 6. At the inlet only the conditions in cooling channel four are measured, the remaining channels are assumed to have equal inlet properties. However, each cooling channel hast dedicated temperature and absolute pressure sensors at its outlet. Furthermore the differential pressure is recorded for all cooling channels between the locations indicated in Figure 6. The mass flow rate of each cooling channel is determined

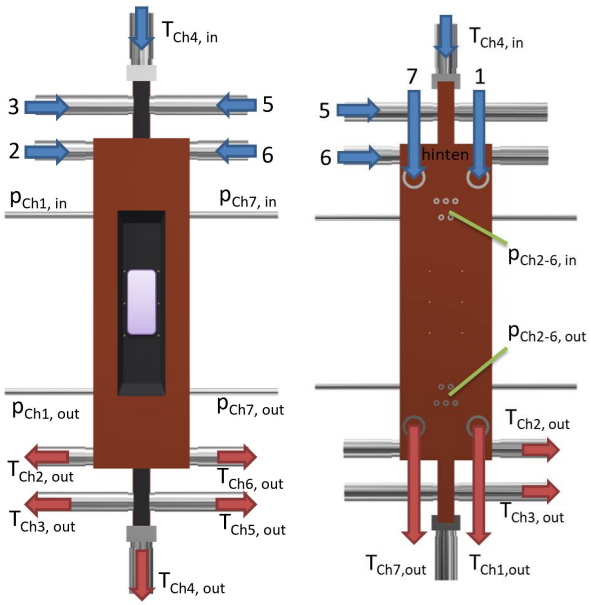

(a) Front side sensor locations (b) Back side sensor locations

Figure 6: **Overview of sensor locations on HTT panel**

via seven EMERSON Coriolis flow meters with an accuracy of $\pm 0.5\%$ of the measured value.

During the laser-on period the 2-dimensional surface

temperature is measured by a FLIR SC7600 infrared (IR) camera with a resolution of 640 x 512 pixels at a wavelength $\lambda_{IR} = 3.99\ \mu\text{m}$. The frame rate is $f_{IR} = 4$ Hz. In order to prevent the influence of reflected laser light a high pass filter ($\lambda_{hp} = 2.5\ \mu\text{m}$) made of Germanium glass is mounted between the panel and the IR camera. The accuracy of the IR camera is ± 1 % or ± 1 K. For the data acquisition and controlling two computers running a LABVIEW software are used. For further details regarding the measurement and control system see [3].

Fluid System

The test bench fluid system is schematically presented in Fig. 7. The nitrogen coolant is a mixture of liquid nitrogen (LN_2, $p = 5$ bar, $T = 94$ K) which is fed into the system by a cryogenic reciprocating pump, and gaseous nitrogen (GN_2, $p = 200$ bar, $T = 288$ K) that is provided by the central supply of the DLR Institute of Space Propulsion. To avoid oscillating mass flow rates induced by the pump it uses two pistons and significant pressure drops are implemented in the fluid system of the test bench. After being mixed the coolant is separated into seven individual cooling channel feed lines. Each of the cooling channels is controllable with a control valve, in order to provide identical mass flow rates within each channel. The maximum achievable mass flow rate per cooling channel is $\hat{\dot{m}}_{cc} = 50$ g/s, the minimum mass flow rate is $\dot{m}_{cc} = 8$ g/s. Behind the HTT panel the coolant is merging inside a collector. This allows the pressure inside the cooling channels to be controlled with a single control valve at the outlet. The coolant is then dumped into the environment.

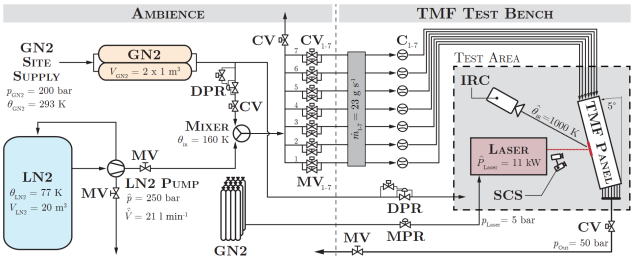

Figure 7: **Schematic of the test bench fluid system as presented by Thiede [3]**

Test Conditions

Each test is defined by the following parameters:

- Temperature of the laser loaded surface T_s
- Heat flux into the HTT panel $\dot{q}_w$

For comparability the outlet pressure of the N_2-coolant is set to $p_{out} = 55 \pm 0.5$ bar. Hence, the resulting pressure difference between laser loaded surface and cooling channel is very close to the pressure difference between the hot gas and the coolant in a real LRE. The inlet temperature of the coolant is typically set to $T_{in} = 160 \pm 2$ K. Thus, the coolant fluid is at supercritical conditions. The mass flow rate per cooling channel that is necessary to achieve the preset conditions is typically determined experimentally by a trial and error approach at the beginning of each TMF panel test within the first 4 - 6 cycles. However, this procedure results in 4 - 6 cycles in which the actual test conditions are differing from the volitional test conditions. The objective of the HTT panel was generating reference data that can be interpolated for a variety of test conditions as well as validation data for coupled CFD/thermal FE analyses. Therefore the surface temperature of the laser loaded area was varied between $T_{s,min} = 648 \pm 1$ K and $T_{s,max} = 1000 \pm 1$ K in increments of $\Delta T_s \approx 120$ K. The heat flux into the laser loaded surface of the HTT panel was varied between $\dot{q}_{w,min} = 12\ \text{MW/m}^2$ and $\dot{q}_{w,max} = 24.6\ \text{MW/m}^2$. The most efficient methodology was to adjust the same value for the mass flow rate in each cooling channel ($\Delta \dot{m}_{cc} = \pm 0.3$ g/s) and then increase the laser output control voltage until the desired surface temperature is met. With Equation (2) the applied heat flux can be determined. The laser-on time consists of a ramp-up of $t_{up} = 30$ s, a holding time of $t_{hold} = 200$ s were steady state conditions are met (see Fig. 11), and a ramp-down of $t_{down} = 30$ s. The time between two laser-on times was long enough (>10 minutes) to allow the HTT panel to completely cool down to the pre-cooling condition of $T = 160$ K again.

3. Theoretical Background

This section describes the most important physical relations which are used for the evaluation of the test results. These are the inward rate of heat flow $\dot{Q}_{in}$ by laser radiation, the outward rate of heat flow $\dot{Q}_{out}$ that is transported in the fluid as well as the Nusselt correlations for determination of the heat transfer coefficient.

3.1 Heat Flow Rate

The inward rate of heat flow depends on the optical output power P of the laser and the emissivity coefficient of the HTT panel coating $\varepsilon(\lambda, T)$ which generally depends on the wavelength of the laser and the temperature of the HTT panel surface. However, for the specific coating used here the emissivity for $\lambda_{laser} = 940$ nm is adequately approximated by neglecting the dependency on temperature. The following equation is applied for the inward rate of heat flow

$$\dot{Q}_{in} = P\varepsilon_{940\ \text{nm}}. \tag{3}$$

The outward rate of heat flow is determined calorically by calculating the enthalpy difference ΔH of the N_2 coolant between the inlet and outlet

$$\dot{Q}_{out} = \sum_{i=1}^{7} \dot{m}_{cc,i} \left(h_{out,i} - h_{in,i}\right). \tag{4}$$

3.2 Heat Transfer Coefficient and Nusselt Correlation

The definition of the convective heat transfer coefficient α with respect to the heat flux $\dot{q}$ is

$$\dot{q} = \alpha\,(T_w - T_b) \tag{5}$$

T_w is the wall temperature on the fluid side and T_b is the bulk temperature of the fluid. T_w was evaluated by a 3-dimensional steady-state thermal FE analysis in ANSYS Mechanical to account for the asymmetrical heating of the cooling channels in the test setup (and also in LRE's). Input conditions were the specific combinations of measured surface temperature and laser-induced heat flux taken from the experimental data. The wall temperature for the Nusselt correlations was determined by averaging the temperature along the circumference of the central cooling channel at the cross-section plane of the point of maximum temperature of the HTT panel.

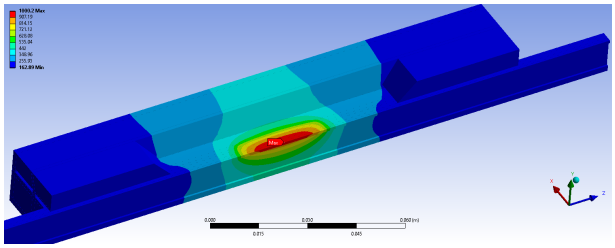

Figure 8: **Steady-state thermal FE analysis of the HTT panel for $T_s = 1000$ K and $\dot{q} = 24.6\ \mathrm{MW/m^2}$**

The definition of the dimensionless Nusselt number Nu, describing the ratio of convective to conductive heat transfer in a fluid, is

$$Nu = \frac{\alpha D_h^*}{\lambda_{fl}} \tag{6}$$

with λ_{fl} describing the heat conductivity of the fluid and D_h^* is effective hydraulic diameter calculated by

$$D_h^* = \phi^* D_h \tag{7}$$

where D_h is the hydraulic diameter

$$D_h = \frac{4A_{cc}}{P_{cc}} = \frac{2lw}{l+w} \tag{8}$$

with A_{cc} being the cross section, P_{cc} is the perimeter and l and w denote the height and width of the cooling channel, respectively. ϕ^* is defined by

$$\phi^* = \frac{2}{3}\left(1+\frac{w}{l}\right)^2\left(1 - \frac{192w}{\pi^5 l}\sum_{n=0}^{\infty}\frac{\tanh\left(\frac{(2n+1)\pi l}{2w}\right)}{2n+1}\right) \tag{9}$$

according to the effective Reynolds Number introduced by Jones in [7] for rectangular cross sections. The effective Reynolds Number is calculated by

$$Re_{eff}^* = \frac{\rho u D_h^*}{\eta} \tag{10}$$

and with $\dot{m} = \rho A_{cc} u$ by

$$Re_{eff}^* = \frac{\dot{m} D_h^*}{A_{cc}\eta}. \tag{11}$$

Note that the effective Reynolds number Re_{eff}^* is used throughout the paper but for convenience denoted as Re. Generally, Nusselt number correlations for forced convection are functions of the Reynolds number and the Prandtl number

$$Nu = Nu(Re, Pr) \tag{12}$$

with

$$Pr = \frac{\eta c_p}{\lambda} \tag{13}$$

The Dittus-Boelter-Equation [8] (14)

$$Nu = 0.023 Re^{0.8} Pr^n \tag{14}$$

is a simple and well known correlation for turbulent flow in smooth tubes. The exponent is $n = 0.3$ for the fluid being cooled and $n = 0.4$ for the fluid being heated. It serves as a basic equation for many correlations of the Nusselt number. However, there are numerous variations for Nusselt correlations evaluated in different research publications. Each is well suited for specific boundary conditions and therefore has to be chosen carefully. Following, some common Nusselt correlations for the heat transfer in liquid rocket engines are evaluated for the test case presented here. It has to be noted, that most of these correlations were developed for supercritical hydrogen or helium, though supercritical nitrogen was used as a coolant here. Only the correlation by Perkins and Worsoe-Schmidt [9] (Equation 15) was found to be appropriate here as an example for a Nusselt correlation with nitrogen as fluid.

One of the most important aspects for the Nusselt correlations is the temperature at which the Reynolds and Prandtl number are evaluated. While the coefficients of the Dittus-Boelter-Equation (14), the Perkins and Worsoe-Schmidt (15) correlation

$$Nu = 0.024 Re^{0.8} Pr^{0.4}\left(\frac{T_w}{T_b}\right)^{-0.7} \tag{15}$$

as well as the correlation by McCarthy and Wolf [10] (16)

$$Nu = 0.023 Re^{0.8} Pr^{0.4}\left(\frac{T_w}{T_b}\right)^{-0.3} \tag{16}$$

are calculated using the bulk temperature T_b, several other concepts have been published. Perkins and Worsoe-Schmidt (15) and McCarthy and Wolf (16) extended the Dittus-Boelter equation by the quotient of the inner wall temperature T_w and the bulk temperature of the fluid T_b. The correlation by Hess and Kunz [11] (17)

$$Nu = 0.0208 Re_f^{0.8} Pr_f^{0.4}\left(1 + 0.01457\frac{\nu_w}{\nu_b}\right) \tag{17}$$

uses the film temperature

$$T_f = \frac{T_w + T_b}{2} \tag{18}$$

for evaluation of Re and Pr for supercritical hydrogen and the quotient of the kinematic viscosity for the conditions at the wall ν_w and the bulk conditions ν_b. Another concept is using the reference temperature

$$T_{0.4} = T_b + 0.4\,(T_w - T_b) \tag{19}$$

developed by Miller, Seader & Trebes [12] (20)

$$Nu = 0.0204 Re_{0.4}^{0.8} Pr_{0.4}^{0.4} \left(1 + 0.00983 \frac{\nu_w}{\nu_b}\right) \tag{20}$$

for evaluation of the Reynolds and Prandtl numbers for a turbulent hydrogen flow.

4. Results

Figure 9 shows the results obtained for the dependency of the coolant mass flow rate on heat flux and surface temperature. The Reynolds number at inlet conditions Re_{in} on the abscissa was chosen instead of the mass flow as this compensates the tolerances of inlet temperature and pressure of the coolant adequately. The data was evaluated at a laser-on time of $t = 220$ s (including 30 s of ramp-up). At this time the test setup has reached steady state conditions (see Fig. 11) making the results easily comparable.

The curves for constant temperature also indicate, that

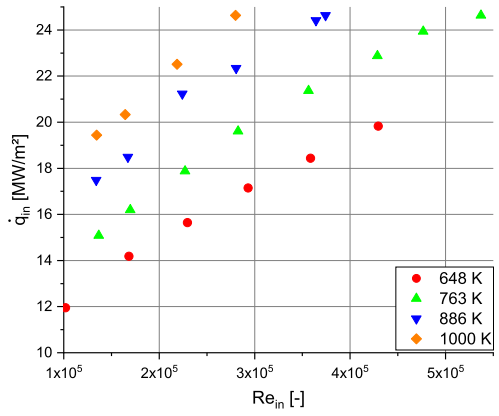

Figure 9: **Heat flux of the laser against the Reynolds numbers at the HTT panel inlet conditions.**

for high Reynolds numbers the slope is not constant, particularly visible in Fig. 9 for $T_s = 763$ K. Consequently the mass flow needs to be increased non-linearly when increasing the heat flux. This rises the question, if there is a limit for the current test setup, where the heat flux can not be increased any further while keeping the surface temperature constant even though the mass flow is increased.

With the help of Figure 9 it is now possible to directly predict the necessary mass flow for different combinations of heat flux and surface temperature for all the following test campaigns in the current project by interpolation.

Figure 10 shows the normalized difference between

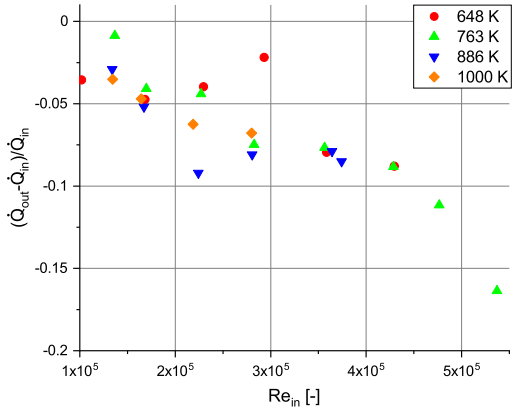

Figure 10: **Normalized difference of the heat flow rate between calculated laser input and measured outflow.**

the caloric outward and applied inward heat flow rate depending on the Reynolds number at inlet conditions. Most of the points are in the order of $\Delta\dot{Q} < -10\%$. This difference is reasonably explainable with the heat conduction from the HTT panel into the fluid supply system. A clear indication for this is the increase of the inlet temperature by $\Delta T_{in} \approx 4$ K (for $T_s = 1000$ K, $\dot{q}_w = 24.6$ MW/m^2) during a laser on cycle as seen in Figure 11. Additionally, some heat is lost through radiation,

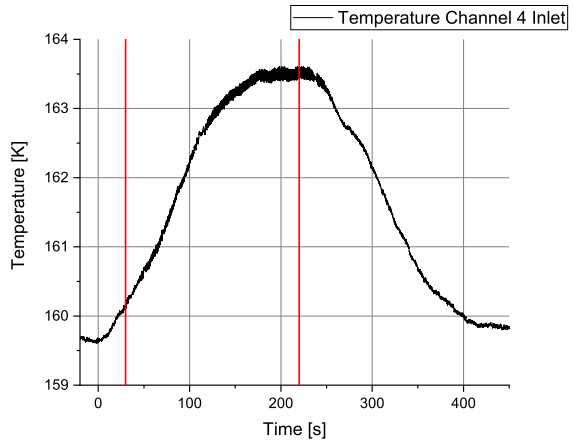

Figure 11: **Evolution of the fluid inlet temperature in cooling channel 4 during a laser cycle. The red bars mark the laser holding time $t_{hold} = 200$ s.**

particularly from the laser heated area. For the validation of a CFD and thermal FE simulation this effect needs to be taken into account.

Figure 12 - 15 visualize the previously presented different Nusselt correlations (see Chapter 3.2) over the corresponding inlet Reynolds number for each temperature. Additionally, the results of the processed experimental data are presented. For the experimental Nusselt number the wall temperature that was identified within the steady-state thermal FE analysis is used. This FE anal-

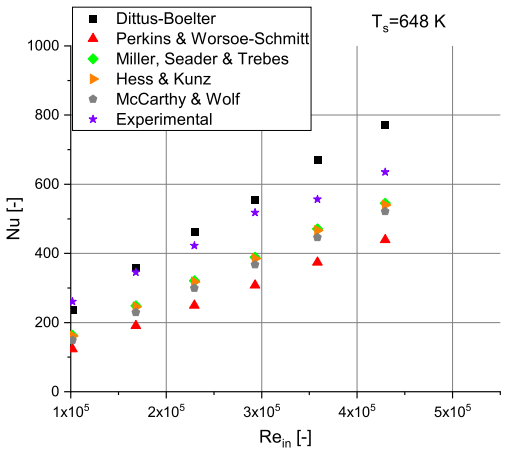

Figure 12: Results of Nusselt correlations for $T_s = 648$ K

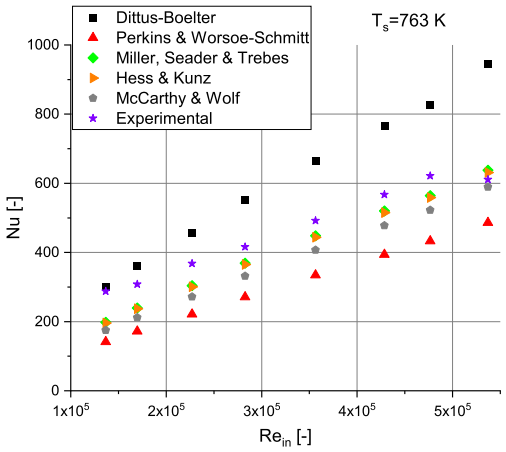

Figure 13: Results of Nusselt correlations for $T_s = 763$ K

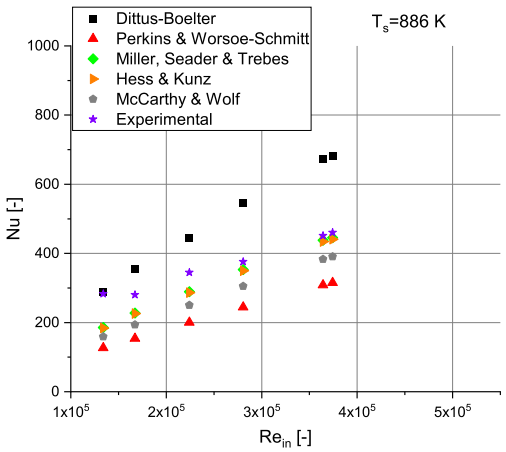

Figure 14: Results of Nusselt correlations for $T_s = 886$ K

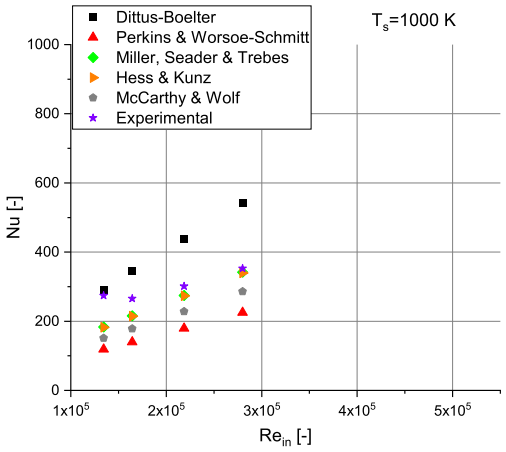

Figure 15: Results of Nusselt correlations for $T_s = 1000$ K

ysis accounts for the asymmetrical heating of the cooling channel and had to be applied since no temperature measurements inside the wall structure, like Woschnak [13] and Haemisch [14] performed, were possible for the HTT panel. The correlations by Miller, Seader & Trebes (Equ. (20)) and Hess & Kunz (Equ. (17)) provide almost identical results for each temperature, even though they used different temperatures for the evaluation of the fluid properties in the Reynolds and Prandtl number. The Dittus-Boelter correlation (Equ. (14)) delivers the highest Nusselt numbers and overall seems to be an inappropriate approach for predicting the heat transfer in the HTT panel, though it is in good accordance with the experimentally determined Nusselt numbers for $Re_{in} < 1.5{\times}10^5$ and most data points with $T_s = 648$ K. For $Re_{in} > 1.5{\times}10^5$ the experimental Nusselt number is well represented by the correlations by Miller, Seader & Trebes and Hess & Kunz, though they provide constantly smaller values. The remaining correlations by McCarthy & Wolf (Equ. (16)) and Perkins & Worsoe-Schmitt (Equ. (15)) predict even lower values for the Nusselt number with the latter being the smallest, around 25% smaller than Miller, Seader & Trebes and Hess & Kunz. While the curves of the correlations evaluated here all show a constant slope, the experimental Nusselt numbers do not. Particularly for small Nusselt numbers around $Re_{in} \approx 1.5 \times 10^5$ and Figures 14 and 15 one can see that the slope is almost constant.

5. Discussion

The results presented in Figures 9 and 10 meet the expectations. Though it has to be considered, that high pressure LREs generally have higher heat fluxes than the laser used here can provide. However, the HTT panel is a valuable approach on the heat transfer for the test setup and validation of simulations within the context of this project. It has to be noted, that the different Nusselt correlations have been developed for cases with different boundary conditions. Like already mentioned in Chapter 3.2, supercritical hydrogen or helium were mostly used. Another important aspect on heat transfer is the asymmetric heating of cooling channels in LREs, which is also well represented within the HTT panel experimental setup but not considered in the examined correlations here (full periphery heating [15]). However, the asymmetrical heating of the cooling channels in the HTT panel is taken into account by the 3-dimensional

(FE analysis) processing of the experimental data, since the circumferential averaged wall temperature is used for the Nusselt number in this case. Additionally, the Nusselt correlations were developed for tubular cooling channels with circular cross sections whereas a rectangular channel is used in LREs. This is accounted for in Equation (7). The values of the examined Nusselt correlations are, with the exception of the Dittus-Boelter correlation, smaller than the experimental Nusselt numbers with a wall temperature processed by a 3-dimensional steady-state FE analysis. However, the absolute difference among the individual values is still quite large. In order to receive a robust prediction on the heat transfer, particularly the numerical simulation needs to be improved. The values for the convective heat transfer coefficient α determined by the simulation are much smaller because these are representing the a mean value along the cooling channel and therefore not presented. The focus in the study presented in this manuscript only focuses on the plane were the maximum temperature occurs. It also has to be noted that the axial heat conduction in the fluid as well as in the HTT panel is not accounted for in the results for the experimental Nusselt number. Axial heat conduction becomes more important for small Reynolds numbers as the fluid velocity is low. This is probably the main cause for the non-constant slope for the experimental Nusselt number.

6. Summary

The results for the dependency of coolant mass flow rate on heat flux and surface temperature for the Heat Transfer Test Panel were presented in this paper. These results are valuable for the following thermomechanical fatigue study on this particular potential inner liner material for a LRE. It will provide essential data to validate a coupled FEM-CFD (thermal FSI analysis) simulation. All test objectives were met. Additionally, different Nusselt correlations have been examined with the data gained in the experiments, processed by a 3-dimensional steady-state thermal FE analysis approach for determination of the wall temperature in the cooling channel.

7. Outlook

The experimental work presented here serves as the basis for the heat transfer analysis of a thermomechanical fatigue life study for a LRE combustion chamber made of high thermal conductivity copper. It allows to quickly adjust the mass flow rate for a variety of combinations of heat flux and surface temperature without the need to use an iterative approach. The results of these following TMF panel experiments will be presented later. Since in the results for the evaluation of the Nusselt number presented here only a very simple 3-dimensional thermal FE analysis was used, there is still a wide potential for improvement. Since at the point of evaluation of the Nusselt number the thermal boundary layer is not fully developed, this effect needs to be considered in future analyses. As a first step, a coupled thermal FE + CFD simulation (thermal FSI analysis) will be set up and compared to the approach used here. Further experimental studies should include the determination of the friction coefficient inside the cooling channels like done in some previous work by the authors [2].

Acknowledgments

The authors thank the European Space Agency (ESA) for funding and Dr. Gordan Thiede for his work at the early stages of the project. Furthermore the authors would like to express their gratitude to Prof. Dr.-Ing. Thomas Seifert, Hochschule Offenbach, and Dr. Christoph Schweizer, Fraunhofer IWM Freiburg, for determination of the material parameters as well as Sebastian Kahl for maintaining the TMF test bench and supporting operations.

References

[1] J. Riccius et al., "TMF: Laser Application for a Close-to-Reality Simulation of Thermo-Mechanical Fatigue Processes in Rocket Engines," in 2nd European Conference for Aero-Space Sciences (EUCASS), 2007.

[2] A. Gernoth, "Untersuchung der Turbulenzmodellierung von rauen Rechteckkanalströmungen mit Berücksichtigung der Oberflächenverformung im Hinblick auf die Anwendung in Raketenmotoren." PhD thesis, University of Stuttgart, 2013.

[3] R. G. Thiede, "Validation of Damage Parameter Based Finite Element Fatigue Life Analysis Results to Combustion Chamber Type Thermomechanical Fatigue Panel Tests," PhD thesis, RWTH Aachen University, 2019.

[4] P. H. Kringe, J. R. Riccius, and M. Oschwald, "Low-cost life assessment of liquid rocket engines by replacing full-scale engine tests with TMF panel tests," Journal of the British Interplanetary Society, vol. 73, no. 5, pp. 152-162, May 2020.

[5] G. Waxenegger-Wilfing, K. Dresia, J. C. Deeken, and M. Oschwald, "Heat Transfer Prediction for Methane in Regenerative Cooling Channels with Neural Networks" Journal of Thermophysics and Heat Transfer Vol. 34, No. 2, April?June 2020. https://doi.org/10.2514/1.T5865

[6] A. Gernoth, J. Riccius, O. Haidn, L. Brummer, B. Mewes, and K. Quering, "TMF panel tests: close-to-reality simulation of thermo-mechanical fatigue processes in heat-loaded walls," in 44th AIAA/ASME/SAE/ASEE Joint Propulsion Conference and Exhibit, 2008, no. [5237].

[7] O. C. Jones Jr., "An improvement in the calculation of turbulent friction in rectangular ducts," In: Journal of Fluids Engineering 98 (1976), pp. 173-181.

[8] F. W. Dittus and L. M. K. Boelter, "Heat transfer in automobile radiators of the tubular type". University of California Press, (1930)

[9] H. C. Perkins and P. Worsoe-Schmidt: "Turbulent heat and momentum transfer for gases in a circular tube at wall-to-bulk temperature ratios to seven". In: Technical Report SU247-7 (1964)

[10] J. R. McCarthy and H. Wolf, "Forced Convection Heat Transfer to Gaseous Hydrogen at High Heat Flux and High Pressure in a Smooth, Round, Electrically Heated Tube", ARS Journal, Vol. 30, April 1960, pp. 423-424.

[11] H. L. Hess and H. R. Kunz, "A Study of Forced Convection Heat Transfer to Supercritical Hydrogen", Journal of Heat Transfer, Vol. 87, No. 2, 1965, pp. 41-48.

[12] W. S. Miller, J. D. Seader and D. M. Trebes, "Forced Convection Heat Transfer to Liquid Hydrogen at Supercritical Pressures," International Institute of Refrigeration, Grenoble, France, June 1965.

[13] A. Woschnak, "Untersuchung des Wärmeübergangs in regenerativ gekühlten Schubkammern kryogener Raketentriebwerke." Dissertation, PhD thesis, RWTH Aachen University, 2009.

[14] J. Haemisch, "Heat Transfer Processes for Hydrogen and Methane in Cooling Channels of Regeneratively Cooled Thrust Chambers of Cryogenic Rocket Engines." PhD thesis, RWTH Aachen University, 2020.

[15] Y. Torres, "Heat and Mass Transfers in Curved Cooling Channels of Rocket Engines." PhD thesis, L´Université de Valenciennes et du Hainaut Cambrésis, 2008.